論文 / 著書情報
Article / Book Information

Title	Impact of Ionic Conduction on Hysteresis and Long-Term Degradation in Perovskite Solar Cells
Authors	Ryotaro Fukuda, Takahito Nishimura, Ming-Hsuan Yu, Chu-Chen Chueh, Akira Yamada
Citation	ACS Applied Energy Materials, Vol. 8, Issue 2, pp. 759-766
Pub. date	2025, 1
DOI	https://doi.org/10.1021/acsaem.4c01993
Creative Commons	Information is in the article.

ACS APPLIED ENERGY MATERIALS

www.acsaem.org

Article

Impact of Ionic Conduction on Hysteresis and Long-Term Degradation in Perovskite Solar Cells

Ryotaro Fukuda,* Takahito Nishimura, Ming-Hsuan Yu, Chu-Chen Chueh, and Akira Yamada*

Cite This: ACS Appl. Energy Mater. 2025, 8, 759−766

Read Online

ACCESS | Metrics & More | Article Recommendations | Supporting Information

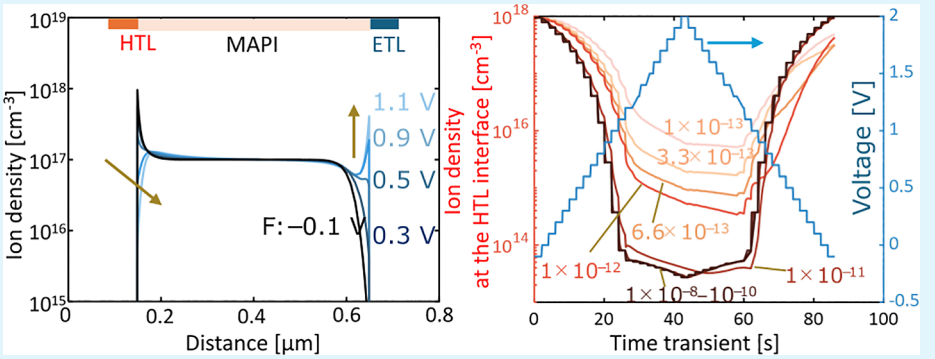

ABSTRACT: Perovskite solar cells, known for their high efficiency, face a challenge with hysteresis in current−voltage (J−V) measurements, complicating accurate characterization. This study explores the factors contributing to hysteresis, with a particular focus on ionic conduction, to address this issue. We have developed an analytical model incorporating transient response analysis to reproduce hysteresis and evaluate the impact of ionic parameters such as mobility and interfacial recombination. Our findings identified iodine vacancy (V_I) conduction as a primary cause of J−V hysteresis, offering significant insights for the field. We also discovered that methylammonium vacancies (V_{MA}) contributed to long-term cell performance degradation, with diffusion coefficients higher than previously reported. This research highlights the practical importance of understanding ionic conduction to improve the characterization and efficiency of perovskite solar cells, emphasizing the need for further investigation in this area.

KEYWORDS: *perovskite, solar cell, ion-diffusion, hysteresis, degradation*

1. INTRODUCTION

Perovskites have attracted considerable attention as a highly efficient thin-film solar cell material, achieving efficiencies exceeding 25% owing to frequent updates in peak conversion efficiencies over the past decades.[1,2] However, one of the critical challenges in these devices is the hysteresis observed in current−voltage (J−V) measurements, which complicates accurate performance evaluation.[3,4] Unlike technologies such as silicon or CIGS solar cells, hysteresis is a prominent issue in perovskite cells. Additionally, the introduction of mesoporous TiO_2 layers, fullerene electron transport layers, and SnO_2 layers has been found to reduce hysteresis, resulting in higher cell efficiencies.[5,6] This trend suggests a strong correlation between hysteresis and conversion efficiency.

Understanding the factors contributing to hysteresis is crucial for developing stable perovskite solar cells. Ion conduction, dielectric properties,[7] and defect-mediated carrier traps[8] have been identified as key contributors, with ion conduction playing a central role. The conduction mechanism of V_I is driven primarily by vacancy-mediated diffusion, where I^- ions migrate along the octahedral edges, benefiting from a lower activation energy compared to Pb^{2+} and $CH_3NH_3^+$ ions, plays a key role in the observed J−V hysteresis.[9] While density functional theory (DFT) calculations and experimental measurements have provided estimates of diffusion coefficients for these ions, the reported values vary significantly. It indicates a need for further investigation into their precise roles.[9−14]

Interfacial properties also have a strong influence on hysteresis, particularly through their impact on recombination processes.[15−18] In this study, we adopt a dynamic ion conduction model to analyze the effects of mobile ions on hysteresis and long-term degradation in perovskite solar cells, with a focus on the interplay between carrier concentration and interfacial recombination. While several studies have examined the relationship between ion conduction and hysteresis, few

Received: August 5, 2024
Revised: December 25, 2024
Accepted: December 30, 2024
Published: January 9, 2025

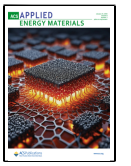

have explored the transient response of reversible long-term degradation under solar illumination.[19,20]

By combining hysteresis analysis with transient response modeling,[21−28] this research provides new insights into the dynamic processes governing both hysteresis and long-term degradation in perovskite solar cells. These findings contribute to a deeper understanding of ion migration, recombination dynamics, and their implications for device stability, offering valuable perspectives for improving the long-term performance of perovskite solar cells.

2. EXPERIMENTAL METHODS

Figure S1 shows the results of $J-V$ measurements for the perovskite solar cell employing an ITO/poly[bis(4-phenyl)(2,4,6-trimethylphenyl)amine] (HTL)/MAPI/phenyl-C61-butyric acid methyl ester (ETL)/Bathocuproine (BCP)/Ag structure. The MAPI films were deposited via spin coating.[18] The solar cell structure and fabrication process were similar to existing samples, achieving an efficiency of more than 18%. However, in this study, the ETL films were thinner (7 nm) compared to the 20−40 nm typically used by other researchers[29−31] to enhance the observation of interface recombination effects. For $J-V$ measurements, the voltage was increased from −0.5 to 2 V at a rate of 0.05 V s^{-1} and subsequently reduced from 2 V back to −0.5 V at the same rate. A comparison between the red line representing the forward direction and the blue line representing the reverse direction reveals significant hysteresis. Specifically, the current in the reverse direction surpassed that in the forward direction for applied voltages between 0 and 0.5 V. Conversely, for applied voltages exceeding 0.5 V, the current in the forward direction exceeded that in the reverse direction. While the short-circuit current density (J_{SC}) for the forward and reverse directions was the same, there was a difference in the open-circuit voltage (V_{OC}).

To assess the impact of this hysteresis, the $J-V$ characteristics were calculated using Silvaco's ATLAS device simulator software.[32] Figure S2 shows the simulated structure of the perovskite solar cell, featuring an ITO/PTAA (HTL)/MAPI/PCBM (ETL)/Ag configuration. The parameters are summarized in Table S1. To delineate and analyze the effects of interfacial recombination, the model initially excluded interfacial defects at the HTL/MAPI and MAPI/ETL interfaces in the first part of this discussion. In the latter part, the model was adjusted to include interfacial defects with equal hole and electron capture cross sections by varying defect density. For simplicity, only V_I and V_{MA} were considered as the positive ions and negative ions, with diffusion coefficients of 1×10^{-12} ($D_{positive}$) and 1×10^{-16} cm^2 s^{-1} ($D_{negative}$), respectively.[9]

The calculations for the $J-V$ measurements proceeded as follows. First, positive and negative ions were distributed uniformly throughout the MAPI film at 1×10^{17} cm^{-3} concentrations. Subsequently, a time-transient simulation was conducted over 10,000 s under dark conditions to achieve a steady-state ion distribution. The ion distribution state established after 10,000 s was used as the initial condition for the time-dependent $J-V$ simulation. Next, solar irradiation (AM1.5) was initiated from the HTL side, and the applied voltage was adjusted to −0.1 V. From this initial state, the applied voltage was incrementally increased from −0.1 to 2 V and similarly decreased from 2 to −0.1 V, with each voltage step being 0.1 V. The time evolution of the current and ion distribution was calculated for 2 s after each voltage step, and the current at the end of this simulation step was taken as the current at the respective applied bias voltage.

3. RESULT

3.1. Investigating the Role of Positive Ions in Hysteresis of Perovskite Solar Cells. Figure 1 depicts the $J-V$ curves calculated by the simulation model under AM 1.5 irradiation. The current density for the reverse direction (blue line) surpasses that for the forward direction (red line) at a bias voltage of approximately 1 V. This calculation excluded interfacial defects at the HTL/MAPI and MAPI/ETL interfaces. To investigate the cause of this hysteresis, the evolution of ion distribution during the $J-V$ measurements was carefully analyzed. Figure 2a illustrates the transition of positive ion distribution during the forward direction from −0.1 to 1.1 V (near V_{OC}). The darkest blue line is ion distribution at −0.1 V (F: −0.1 V), while the lightest blue line is ion distribution at 1.1 V (F: 1.1 V).

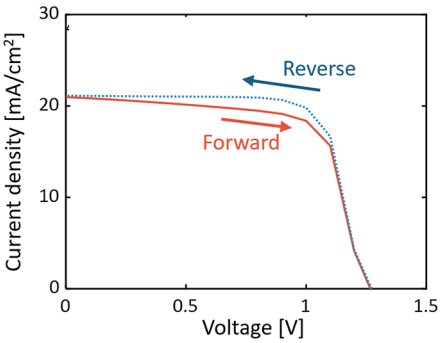

Figure 1. $J-V$ curves calculated by the simulation model. This calculation does not consider interfacial recombination of HTL/MAPI and MAPI/ETL.

In a conventional perovskite solar cell, there is an electric field from the ETL to the HTL in the MAPI layer. However, if mobile ions are present in the MAPI, positive ions accumulate at the HTL/MAPI interface. Eventually, the redistribution of these positive ions neutralizes the electric field, rendering the electric field strength in the central part of the MAPI layer negligible. These conditions are illustrated in Figure 2a (positive ion distribution), Figure 3a (band structure), and Figure 3b (electron−hole concentration) at F: −0.1 V (near-zero bias condition). Under this bias condition, significant electric fields exist at the HTL/MAPI interface, as depicted in Figure 3a, facilitating hole extraction to the HTL, resulting in a significant reduction in hole concentration at the interface, with holes diffusing from the interior of the MAPI layer, as illustrated in Figure 3b. Similar phenomena occur at the ETL/MAPI interface. Eventually, a steady photocurrent flows through the solar cell despite the negligible electric field in the absorber layer. It was observed that electron and hole concentrations were almost equal at the center of the absorber layer. As the applied voltage increases, the positive ions accumulated at the HTL/MAPI interface start to accumulate on the ETL/MAPI side. Consequently, increasing the applied voltage decreases the positive ion concentration at the HTL/MAPI interface and increases it on the ETL/MAPI side. This redistribution of ions occurs due to changes in the electric field within the MAPI layer as the applied voltage increases, causing the ions to reconfigure according to the altered electric field, as seen in Figure 2a.

The blue line in Figure 2b shows the distribution of positive ions near V_{OC} during the reverse direction (R: 1.1 V). R: 1.1 V is the situation 36 s after F: 1.1 V. Comparing F: 1.1 V and R: 1.1 V, differences in positive ion distribution are observed at the MAPI/ETL interface and the HTL/MAPI interface. Therefore, the time variation of ion concentration was examined to assess the time constant of positive and negative ion migrations. In the simulation, the applied voltage was increased from 0 to 0.1 V, and the temporal changes in ion

https://doi.org/10.1021/acsaem.4c01993
ACS Appl. Energy Mater. 2025, 8, 759−766

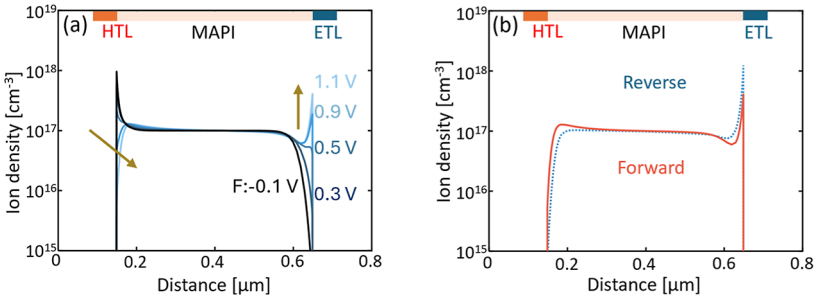

Figure 2. Time-dependent evolution of positive ion distribution during the $J-V$ measurement. (a) Shows ion distributions for the forward scan from −0.1 V (F: −0.1 V) to 1.1 V (F: 1.1 V). (b) Displays ion distributions at 1.1 V under both the forward (F: 1.1 V, red solid line) and reverse (R: 1.1 V, blue dotted line) conditions.

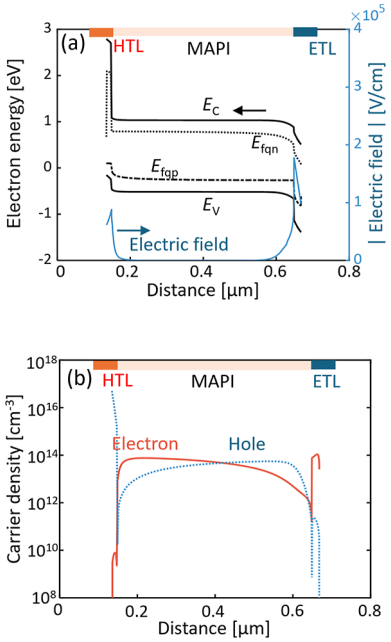

Figure 3. Band structure and electric field (a) and carrier concentration (b) at an applied voltage of −0.1 V. E_{fqn} and E_{fqp} are the quasi-Fermi levels of electrons and holes, respectively.

concentrations at the MAPI/ETL interface were simulated. The results are depicted in Figure 4a. The concentration of negative ions did not vary in this time frame, suggesting that redistribution of negative ions does not occur during $J-V$ measurements. In contrast, the initial concentration of positive ions was 5.3 × 10^{15} cm^{-3}, gradually increasing after applying bias voltage and reaching saturation at 1.3 × 10^{16} cm^{-3} over 30 s. Based on the calculations, the time constant for positive ion migration was estimated to be approximately 10.5 s. The time constant of 10.5 s reflects the response time of positive ions to changes in applied voltage. In our $J-V$ measurements, voltage is increased or decreased at a rate of 0.1 V every 2 s, which is relatively fast compared to the calculated time constant. As a result, positive ions do not fully respond to the voltage changes during the scan, leading to incomplete ion migration and concentration differences between the forward and reverse directions. This incomplete response is illustrated in Figure 4b, where the time evolution of positive ion concentration at the MAPI/HTL interface shows a lag behind the applied voltage. Specifically, the minimum positive ion concentration occurs approximately 16 s after the voltage peak, reflecting a delay in ion migration. For instance, the positive ion concentration at 1 V in the forward direction is approximately 1 × 10^{16} cm^{-3}, while in the reverse direction, it decreases by 1 order of magnitude to less than 1 × 10^{15} cm^{-3}. This variation in positive ion distribution between forward and reverse directions changes the band structure and carrier concentrations and contributes to the observed hysteresis.

Figure 5a shows the band structure at applied voltages F: 1 V and R: 1 V. Figure 5b,d shows the carrier concentration, with the red line representing the forward direction and the blue line representing the reverse direction. Positive ions influence carrier distribution. Accumulation of positive ions increases the electric potential, leading to electron accumulation and

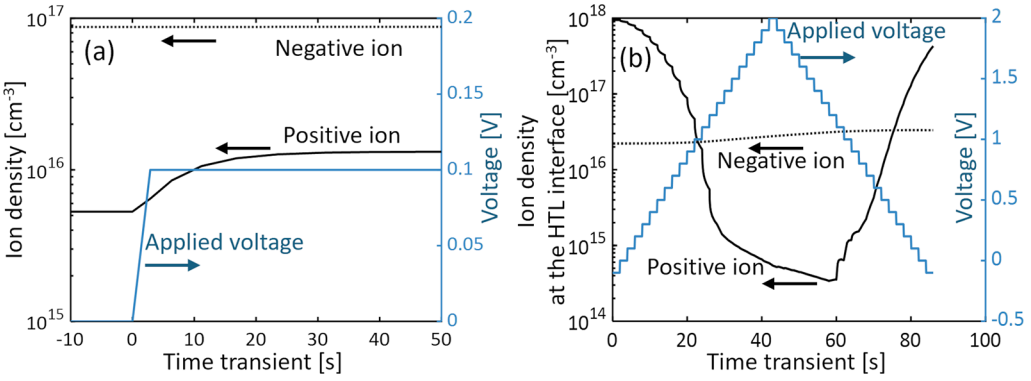

Figure 4. (a) The temporal variation of ion concentrations near the ETL/MAPI interface during the application of a stepwise bias (blue line) to the solar cell. The solid and dotted lines represent the concentrations of positive and negative ions, respectively. (b) The time evolution of positive and negative ion concentrations at the MAPI/HTL interface with the applied voltage during the $J-V$ scan.

https://doi.org/10.1021/acsaem.4c01993
ACS Appl. Energy Mater. 2025, 8, 759−766

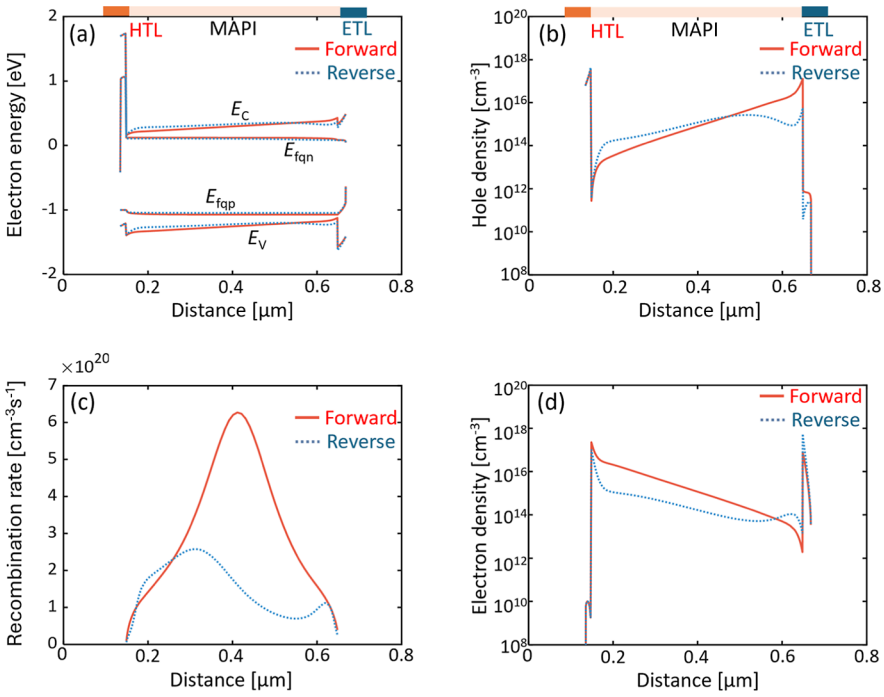

Figure 5. Band structure (a), hole density (b), recombination rate (c), and electron density (d) at a bias voltage of F: 1 V (red line) and R: 1 V (blue line).

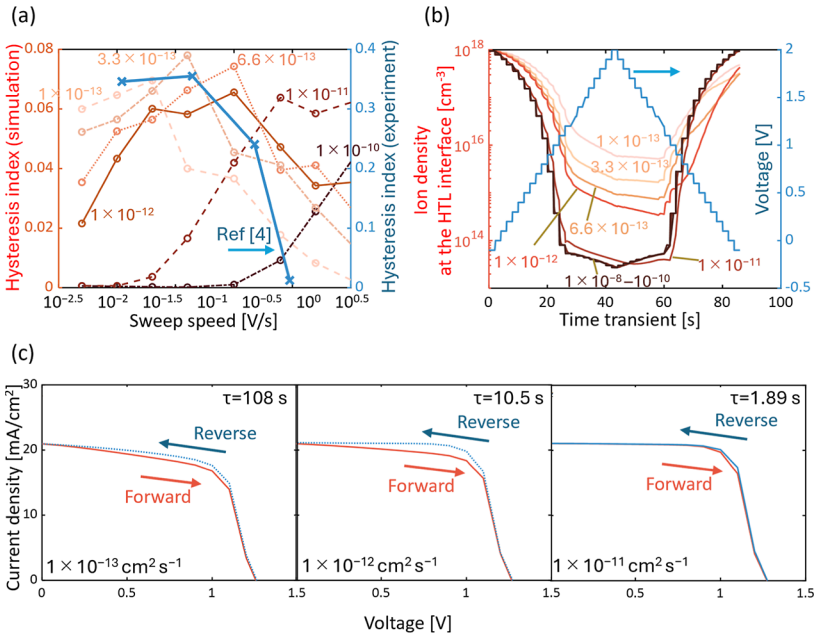

Figure 6. (a) The relationship between hysteresis magnitude and sweep rate for different diffusion coefficients of positive ions. The experimental value was obtained from Snaith's report, while the simulated HI was calculated by varying the diffusion coefficient from 1×10^{-10} to 1×10^{-13} cm^2 s^{-1}. (b) The time evolution of positive ion concentrations at the MAPI/HTL interface with the applied voltage during the $J-V$ scan by varying the diffusion coefficient from 1×10^{-8} to 1×10^{-13} cm^2 s^{-1}. (c) $J-V$ curves for diffusion constants of 1×10^{-13} and 1×10^{-12} and 1×10^{-11} cm^2 s^{-1}.

repulsion of holes. Therefore, the electron concentration at the ETL/MAPI interface is higher in the reverse direction than in the forward direction. In contrast, in the absorber layer, the electron concentration for the reverse direction is lower than that for the forward direction, as depicted in Figure 5b. Notably, there was a significant difference in hole and electron concentrations at the interfaces, and the recombination rate at both interfaces was low. However, in the forward direction, the hole concentration is comparable to the electron concentration at the center of the absorber layer, resulting in a higher recombination rate compared to the reverse direction, as illustrated in Figure 5c. Consequently, the photocurrent in the reverse direction (R: 1 V) was higher than that in the forward direction (F: 1 V).

The above-mentioned calculations strongly corroborate that positive ion (V_I) conduction is responsible for hysteresis. To quantitatively analyze this relationship, we evaluated the hysteresis index (HI) defined by eq 1.[5] In eq 1, J_R

https://doi.org/10.1021/acsaem.4c01993
ACS Appl. Energy Mater. 2025, 8, 759−766

($0.8V_{OC,R}$) is the current value in the reverse direction at an applied voltage of 80% of V_{OC}, and J_F ($0.8V_{OC,F}$) is that in the forward direction.

$$\text{Hysteresis index(HI)} = \left| \frac{J_R(0.8V_{OC,R}) - J_F(0.8V_{OC,F})}{J_R(0.8V_{OC,R})} \right| \quad (1)$$

Based on the experimental results reported by Snaith et al.[4] we calculated the HI values for different scan rates (blue line in Figure 6a). The experimental data show that the HI value peaks at a scan rate of approximately 0.044 V/s. We then performed simulations to calculate the relationship between hysteresis and sweep rate for various diffusion coefficients of positive ions (red lines in Figure 6a). By comparing these theoretical predictions with the experimental results, we estimated the diffusion coefficient of the positive ion to be approximately 3 to 6 × 10^{-13} cm^2 s^{-1}. To further investigate this, we analyzed the time evolution of positive ions concentration at the HTL interface under various diffusion coefficients during $J-V$ scans at a rate of 0.5 V/s. Figure 6b shows the experimental voltage step and corresponding ion density at the HTL interface with various diffusion coefficients. Figure 6c shows the $J-V$ characteristics with a diffusion coefficient of 1 × 10^{-13}, 1 × 10^{-12}, 1 × 10^{-11} cm^2 s^{-1}, respectively. The time constant of ion migration is also shown in the figure. At a high diffusion coefficient (1 × 10^{-11} cm^2 s^{-1}), the positive ions respond rapidly to the applied voltage, leading to small hysteresis due to near-instantaneous ion redistribution. Conversely, with a low diffusion coefficient (1 × 10^{-13} cm^2 s^{-1}), ion migration is too slow to follow the voltage change, resulting in minimal ion redistribution and thus small hysteresis. The maximum hysteresis appears in the intermediate range (3 to 6 × 10^{-13} cm^2 s^{-1}), positive ions exhibit delayed alignment with the applied voltage. This experimentally determined diffusion coefficient of positive ion (V_I) is in good agreement with the value of 1 × 10^{-12} cm^2 s^{-1} predicted by DFT calculations.[9] Although both sufficiently high and low diffusion coefficients result in small hysteresis, the device efficiencies inferred from their respective $J-V$ curves are significantly different. The device shows higher performance when ion conduction can sufficiently follow the voltage change. This finding highlights that the measured performance of perovskite solar cells strongly depends on the ion migration, underscoring the importance of standardized measurement setups.

The diffusion of positive ions successfully reproduces hysteresis. However, the magnitude of the hysteresis observed in the $J-V$ curve calculated in Figure 1 is considerably smaller than that observed in the measurement shown in Figure S1, where the V_{OC} differed between bias directions.

The change in carrier collection efficiency caused by potential differences in the absorber layer has been extensively reported by researchers as a contributing factor to hysteresis.[33,34] However, comparing the band structures calculated in this study reveals that the magnitude of the potential difference in the absorber layer under different bias conditions is only approximately 0.1 eV, as shown in Figure 5a. Therefore, this effect is limited. Furthermore, Rong et al. have suggested that the observed change in V_{OC} in measurements cannot be solely attributed to variations in carrier collection efficiency.[17] They identified the influence of interfacial recombination as the most significant factor affecting the change in V_{OC}. To explore the relationship between interfacial defects and hysteresis response, defects at the ETL/MAPI and MAPI/HTL interfaces were incorporated into the model. The characteristics of these introduced defects are detailed in Table S1.

The simulated $J-V$ curves incorporating interface defects are shown in Figure 7. Compared to the $J-V$ curve without defects

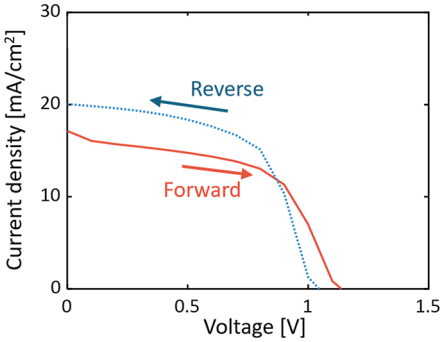

Figure 7. $J-V$ curves calculated using a simulation model incorporating interface defects.

in Figure 3, significant changes are observed in both directions. The difference in V_{OC} values between forward and reverse characteristics is evident in the simulation, resembling the large hysteresis observed in experimental results shown in Figure 1. Interfacial recombination rates were calculated for forward and reverse directions at an applied voltage of 0.9 V to investigate the correlation between V_{OC} difference and interfacial recombination. The calculated recombination rates at the HTL/MAPI and MAPI/ETL interfaces were 5.91 × 10^{22} and 5.75 × 10^{23} cm^{-3} s^{-1} in the forward direction, respectively, while in the reverse direction, these values were 5.16 × 10^{22} and 1.35 × 10^{24} cm^{-3} s^{-1}. The interfacial recombination rate at the MAPI/ETL interface in the reverse direction was 2.34 times higher than that in the forward direction. This increase in recombination rate during the reverse direction results in a decrease in V_{OC}, which contributes to significant hysteresis. Figure S3 shows the ion and carrier concentration distributions at a bias voltage of 0.9 V, highlighting the factors influencing the change in interfacial recombination. In the SRH model, the recombination rate is proportional to the minority carrier concentration, assuming equal hole and electron capture cross sections and low injection conditions. Figure S3b shows that electrons and holes are minority carriers at the MAPI/ETL and HTL/MAPI interfaces, respectively, and they determine the interface recombination rates. The accumulation of positive ions at the MAPI/ETL interface under reverse conditions increased the electron concentration from 1.85 × 10^{11} (forward) to 8.88 × 10^{11} cm^{-3} (reverse). Consequently, the recombination rate more than doubled in the reverse condition, explaining the decrease in V_{OC} owing to the accumulation of positive ions at the ETL/MAPI interface.

3.2. Investigating the Role of Negative Ions in Long-Term Degradation of Perovskite Solar Cells. Thus, far, the impact of negative ions (V_{MA}) has not been addressed. This is attributed to the significantly smaller diffusion coefficient of negative ions compared to positive ions. The distribution of negative ions remains unchanged during the short duration of less than 50 s in $J-V$ measurements, as depicted in Figure 4. However, it has been suggested that slow ion diffusion contributes to the degradation of perovskite solar

https://doi.org/10.1021/acsaem.4c01993
ACS Appl. Energy Mater. 2025, 8, 759−766

cell properties during long-term operation. The association between negative ions and long-term degradation of perovskite solar cells is investigated.

Figure 8a displays the long-term degradation of a perovskite solar cell with an FTO/TiO_2/perovskite/Spiro-OMeTAD/Au

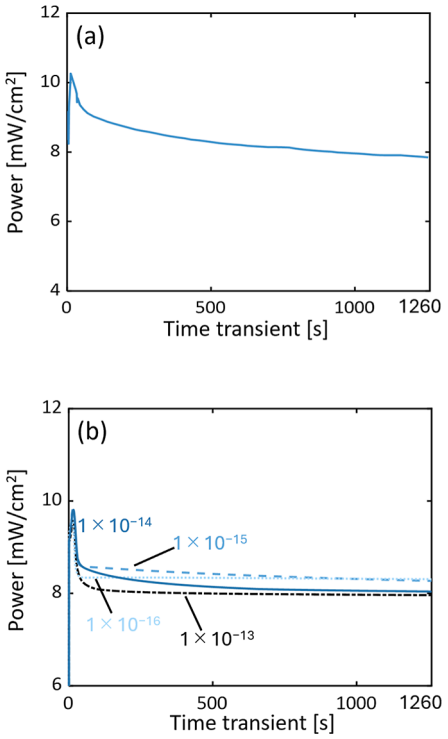

Figure 8. (a) Reported changes in solar cell power generation during 1260 s of sunlight exposure. (b) Calculated power generation changes as a function of the diffusion coefficient of the negative ion. The dotted line shows the calculation results for a 1×10^{-16} cm^2 s^{-1} diffusion coefficient, the dashed line for 1×10^{-15} cm^2 s^{-1}, the solid line for 1×10^{-14} cm^2 s^{-1}, and the chain line for 1×10^{-13} cm^2 s^{-1}. Figure (a) reproduced from ref 19 Copyright 2022 IEEE.

structure, as reported by Tayagaki et al.[19] This figure is reproduced from Figure 2 of his article. After a rapid decline in power generation from 10.3 to 9.2 mW cm^{-2} in the first 45 s, there was gradual property degradation over approximately 1200 s, with power generation decreasing to 7.8 mW cm^{-2} by 1260 s. Power production under solar irradiation (AM1.5) was simulated for 1260 s to reproduce this long-term efficiency degradation using the ionic conduction model. The ETL was switched from PCBM to TiO_2 in the analytical model to mimic the experimental structure, adjusting the band alignment and the carrier concentration.

The long-term variation of the power generation was characterized using the following procedure. The initial dark condition was calculated as described in the previous method. Then, the solar irradiation and the bias voltage were applied. To determine the maximum power point, transient power generation was calculated across 12 bias voltages: 0.45, 0.5, 0.55, 0.65, 0.7, 0.75, 0.8, 0.85, 0.9, 0.95, 1, and 1.05 V for 1260 s, encompassing the range where the maximum power point is expected to occur. After plotting these 12 power generation curves, the long-term power generation curve was estimated by taking the maximum value at each transient time. In the calculations, the diffusion coefficient of the positive ion was set to 2×10^{-12} cm^2 s^{-1}, and the concentration of interfacial defects at the HTL/MAPI and MAPI/ETL interfaces were set to 4×10^{-13} and 1×10^{-13} cm^{-2}, respectively. Figure 8b shows the time-dependent degradation of power generation while varying the diffusion coefficient of the negative ion. The dotted line shows the long-term power generation trend with a negative ion (V_{MA}) diffusion coefficient of 1×10^{-16} cm^2 s^{-1}, estimated via DFT calculations.[9] Following a rapid decline in power production from 9.7 to 8.4 mW cm^{-2} in 30 s, power generation stabilized over 1200 s. The reported long-term degradation in conversion efficiency was not reproduced. However, the dashed and solid lines, corresponding to diffusion coefficients of 1×10^{-15} and 1×10^{-14} cm^2 s^{-1} for negative ions, exhibit a gradual decline in power generation over 1200 s. On the other hand, with a diffusion constant of 1×10^{-13} cm^2 s^{-1} the power generation is again stabilized over 1200 s.

When using a diffusion coefficient of 1×10^{-14} cm^2 s^{-1} for negative ions, the model predicts a decrease in power generation to 8.0 mW cm^{-2} after 1260 s, consistent with the reported value. The observation that the diffusion coefficient of V_{MA} is 10^2 times higher than the theoretical estimate can be explained by the inherent uncertainties in first-principles calculations, where discrepancies of up to 10^2 times are often within the expected range. The sensitivity of the computational models and the parameters used can result in such differences. Additionally, van Reenen et al. have observed a similar mismatch in diffusion coefficients, suggesting that the difference could be due to variations in mobile ion density or the distinct mechanisms of ion transport through the bulk or grain boundaries of the perovskite material.[21] Moreover, Senocrate et al. and Futscher et al. reported experimental values for the V_{MA} diffusion coefficient at 1×10^{-12} cm^2 s^{-1}. This suggests that it is common for the diffusion coefficient values obtained in experiments to be higher than the theoretical values.[10,11] For this model configuration, the calculated interfacial recombination rates were 9.68×10^{22} cm^{-3} s^{-1} at the HTL/MAPI interface and 4.25×10^{23} cm^{-3} s^{-1} at the MAPI/ETL interface after 18 s of initiation at 0.75 V. After 1260 s, the calculated interfacial recombination rates were 2.95×10^{23} (HTL/MAPI) and 3.23×10^{23} cm^{-3} s^{-1} (MAPI/ETL), indicating a more than 3-fold increase in the recombination rate at the HTL/MAPI interface compared to earlier measurements. Figure S4 compares the distribution of positive and negative ions at 18 and 1260 s. It shows that after 1260 s, the HTL/MAPI interface becomes negatively charged, while the MAPI/ETL interface becomes positively charged (Figure S4a). This charging causes the band to shift upward at the HTL interface and downward at the ETL interface, similar to the change in band structure shown in Figure 5a. The energy difference between the quasi-Fermi level of holes and E_V decreases at the HTL/MAPI interface, resulting in nearly triple the hole concentration (minority carrier). Consequently, the interfacial recombination rate at the HTL/MAPI interface increases by more than 3-fold, contributing to the long-term degradation of perovskite solar cells.

4. CONCLUSION

The hysteresis and long-term degradation of perovskite solar cells have been explored through an analytical model incorporating mobile ions in the cell. By analyzing the behaviors of V_I and V_{MA} based on the reported diffusion coefficients, it was determined that the $J-V$ hysteresis primarily results from the conduction of V_I ions. Conversely,

https://doi.org/10.1021/acsaem.4c01993
ACS Appl. Energy Mater. 2025, 8, 759−766

it has been suggested that V_{MA} may contribute to the long-term degradation of cell performance, requiring diffusion coefficients 10^2 times larger than those estimated by DFT. In summary, our study demonstrates that ionic conduction plays a significant role in both hysteresis and the long-term degradation of perovskite solar cells. We emphasize the importance of understanding the impact of ionic conduction for accurately characterizing these solar cells.

■ ASSOCIATED CONTENT

Supporting Information

The Supporting Information is available free of charge at https://pubs.acs.org/doi/10.1021/acsaem.4c01993.

Measured $J-V$ characteristics of a perovskite solar cell; simulation methods for ion diffusion modeling, including equations for ionic conduction and ion mobility; simulated structure of a perovskite solar cell with energy levels, thickness, and doping concentrations; solar cell parameters used in simulations; comparison of ion distributions, charge carrier concentrations, and recombination rates for forward and reverse directions in the model with interface defects introduced; and temporal comparisons of ion and charge distributions during long-term degradation (PDF)

■ AUTHOR INFORMATION

Corresponding Authors

Ryotaro Fukuda − *Department of Electrical and Electronic Engineering, Tokyo Institute of Technology, Tokyo 152-8552, Japan*; orcid.org/0000-0003-3920-4951; Email: fukuda.r.aa@m.titech.ac.jp

Akira Yamada − *Department of Electrical and Electronic Engineering, Tokyo Institute of Technology, Tokyo 152-8552, Japan*; Email: yamada.a.ac@m.titech.ac.jp

Authors

Takahito Nishimura − *Department of Electrical and Electronic Engineering, Tokyo Institute of Technology, Tokyo 152-8552, Japan*

Ming-Hsuan Yu − *Department of Chemical Engineering, National Taiwan University, Taipei 10617, Taiwan*

Chu-Chen Chueh − *Department of Chemical Engineering, National Taiwan University, Taipei 10617, Taiwan*; orcid.org/0000-0003-1203-4227

Complete contact information is available at: https://pubs.acs.org/10.1021/acsaem.4c01993

Notes

The authors declare no competing financial interest.

■ ACKNOWLEDGMENTS

This work was supported by JST SPRING, Grant Number JPMJSP2106.

■ REFERENCES

(1) Green, M. A.; Dunlop, E. D.; Yoshita, M.; Kopidakis, N.; Bothe, K.; Siefer, G.; Hinken, D.; Rauer, M.; Hohl-Ebinger, J.; Hao, X. Solar Cell Efficiency Tables (Version 64). *Prog. Photovoltaics* **2024**, *32* (7), 425−441.

(2) Faini, F.; Larini, V.; Scardina, A.; Grancini, G. Hybrid Halide Perovskites, a Game Changer for Future Solar Energy? *MRS Bull.* **2024**, *49* (10), 1059−1069.

(3) Koide, N.; Han, L. Measuring Methods of Cell Performance of Dye-Sensitized Solar Cells. *Rev. Sci. Instrum.* **2004**, *75* (9), 2828−2831.

(4) Snaith, H. J.; Abate, A.; Ball, J. M.; Eperon, G. E.; Leijtens, T.; Noel, N. K.; Stranks, S. D.; Wang, J. T.-W.; Wojciechowski, K.; Zhang, W. Anomalous Hysteresis in Perovskite Solar Cells. *J. Phys. Chem. Lett.* **2014**, *5* (9), 1511−1515.

(5) Kim, H.-S.; Park, N.-G. Parameters Affecting I−V Hysteresis of CH3NH3PbI3 Perovskite Solar Cells: Effects of Perovskite Crystal Size and Mesoporous TiO2 Layer. *J. Phys. Chem. Lett.* **2014**, *5* (17), 2927−2934.

(6) Zhong, Y.; Hufnagel, M.; Thelakkat, M.; Li, C.; Huettner, S. Role of PCBM in the Suppression of Hysteresis in Perovskite Solar Cells. *Adv. Funct. Mater.* **2020**, *30* (23), 1908920.

(7) Ma, W.; Zhang, X.; Xu, Z.; Guo, H.; Lu, G.; Meng, S. Reducing Anomalous Hysteresis in Perovskite Solar Cells by Suppressing the Interfacial Ferroelectric Order. *ACS Appl. Mater. Interfaces* **2020**, *12* (10), 12275−12284.

(8) van Heerden, R.; Procel, P.; Mazzarella, L.; Santbergen, R.; Isabella, O. Slow Shallow Energy States as the Origin of Hysteresis in Perovskite Solar Cells. *Front. Photonics* **2022**, *3*, 889837.

(9) Eames, C.; Frost, J. M.; Barnes, P. R. F.; O'Regan, B. C.; Walsh, A.; Islam, M. S. Ionic Transport in Hybrid Lead Iodide Perovskite Solar Cells. *Nat. Commun.* **2015**, *6* (1), 7497.

(10) Futscher, M. H.; Lee, J. M.; McGovern, L.; Muscarella, L. A.; Wang, T.; Haider, M. I.; Fakharuddin, A.; Schmidt-Mende, L.; Ehrler, B. Quantification of Ion Migration in CH3NH3PbI3 Perovskite Solar Cells by Transient Capacitance Measurements. *Mater. Horiz.* **2019**, *6* (7), 1497−1503.

(11) Senocrate, A.; Moudrakovski, I.; Kim, G. Y.; Yang, T.-Y.; Gregori, G.; Grätzel, M.; Maier, J. The Nature of Ion Conduction in Methylammonium Lead Iodide: A Multimethod Approach. *Angew. Chem., Int. Ed.* **2017**, *56* (27), 7755−7759.

(12) Li, C.; Guerrero, A.; Huettner, S.; Bisquert, J. Unravelling the Role of Vacancies in Lead Halide Perovskite through Electrical Switching of Photoluminescence. *Nat. Commun.* **2018**, *9* (1), 5113.

(13) Thiesbrummel, J.; Shah, S.; Gutierrez-Partida, E.; Zu, F.; Peña-Camargo, F.; Zeiske, S.; Diekmann, J.; Ye, F.; Peters, K. P.; Brinkmann, K. O.; Caprioglio, P.; Dasgupta, A.; Seo, S.; Adeleye, F. A.; Warby, J.; Jeangros, Q.; Lang, F.; Zhang, S.; Albrecht, S.; Riedl, T.; Armin, A.; Neher, D.; Koch, N.; Wu, Y.; Le Corre, V. M.; Snaith, H.; Stolterfoht, M. Ion-Induced Field Screening as a Dominant Factor in Perovskite Solar Cell Operational Stability. *Nat. Energy* **2024**, *9* (6), 664−676.

(14) Ferdani, D. W.; Johnson, A. L.; Lewis, S. E.; Baker, P. J.; Cameron, P. J. Opposites Attract, Muons as Direct Probes for Iodide Diffusion in Methyl Ammonium Lead Iodide. *arXiv* **2018**, arXiv:1801.03845v2.

(15) Kanlayapattamapong, T.; Thongimboon, K.; Pudkon, W.; Wongratanaphisan, D.; Ruankham, P. Optimizing Thickness of Tin Oxide Electron Transporting Layer to Reduce Hysteresis in Carbon-Based Perovskite Solar Cells. *J. Phys.: Conf. Ser.* **2023**, *2653* (1), 012079.

(16) Yekani, R.; Wang, H.; Bessette, S.; Gauvin, R.; Demopoulos, G. Synergetic Interfacial Conductivity Modulation Dictating Hysteresis Evolution in Perovskite Solar Cells under Operation. *Phys. Chem. Chem. Phys.* **2024**, *26* (10), 8366−8379.

(17) Rong, Y.; Hu, Y.; Ravishankar, S.; Liu, H.; Hou, X.; Sheng, Y.; Mei, A.; Wang, Q.; Li, D.; Xu, M.; Bisquert, J.; Han, H. Tunable Hysteresis Effect for Perovskite Solar Cells. *Energy Environ. Sci.* **2017**, *10* (11), 2383−2391.

(18) Jeon, N. J.; Noh, J. H.; Kim, Y. C.; Yang, W. S.; Ryu, S.; Seok, S. I. Solvent Engineering for High-Performance Inorganic−Organic Hybrid Perovskite Solar Cells. *Nat. Mater.* **2014**, *13* (9), 897−903.

(19) Tayagaki, T.; Kogo, A.; McDonald, C.; Svrcek, V.; Matsui, T.; Yoshita, M. Transient Analysis of Ion-Migration Current for Degradation Diagnostics of Perovskite Solar Cells. *IEEE J. Photovoltaics* **2022**, *12* (5), 1170−1174.

(20) Domanski, K.; Roose, B.; Matsui, T.; Saliba, M.; Turren-Cruz, S.-H.; Correa-Baena, J.-P.; Carmona, C. R.; Richardson, G.; Foster, J. M.; De Angelis, F.; Ball, J. M.; Petrozza, A.; Mine, N.; Nazeeruddin, M. K.; Tress, W.; Grätzel, M.; Steiner, U.; Hagfeldt, A.; Abate, A. Migration of Cations Induces Reversible Performance Losses over Day/Night Cycling in Perovskite Solar Cells. *Energy Environ. Sci.* **2017**, *10* (2), 604−613.
(21) van Reenen, S.; Kemerink, M.; Snaith, H. J. Modeling Anomalous Hysteresis in Perovskite Solar Cells. *J. Phys. Chem. Lett.* **2015**, *6* (19), 3808−3814.
(22) Richardson, G.; O'Kane, S. E. J.; Niemann, R. G.; Peltola, T. A.; Foster, J. M.; Cameron, P. J.; Walker, A. B. Can Slow-Moving Ions Explain Hysteresis in the Current−Voltage Curves of Perovskite Solar Cells? *Energy Environ. Sci.* **2016**, *9* (4), 1476−1485.
(23) Clarke, W.; Cowley, M. V.; Wolf, M. J.; Cameron, P.; Walker, A.; Richardson, G. Inverted Hysteresis as a Diagnostic Tool for Perovskite Solar Cells: Insights from the Drift-Diffusion Model. *J. Appl. Phys.* **2023**, *133* (9), 095001.
(24) Cave, J. M.; Courtier, N. E.; Blakborn, I. A.; Jones, T. W.; Ghosh, D.; Anderson, K. F.; Lin, L.; Dijkhoff, A. A.; Wilson, G. J.; Feron, K.; Saiful Islam, M.; Foster, J. M.; Richardson, G.; Walker, A. B. Deducing Transport Properties of Mobile Vacancies from Perovskite Solar Cell Characteristics. *J. Appl. Phys.* **2020**, *128* (18), 184501.
(25) Bertoluzzi, L.; Boyd, C. C.; Rolston, N.; Xu, J.; Prasanna, R.; O'Regan, B. C.; McGehee, M. D. Mobile Ion Concentration Measurement and Open-Access Band Diagram Simulation Platform for Halide Perovskite Solar Cells. *Joule* **2020**, *4* (1), 109−127.
(26) Neukom, M. T.; Schiller, A.; Züfle, S.; Knapp, E.; Ávila, J.; Pérez-del-Rey, D.; Dreessen, C.; Zanoni, K. P. S.; Sessolo, M.; Bolink, H. J.; Ruhstaller, B. Consistent Device Simulation Model Describing Perovskite Solar Cells in Steady-State, Transient, and Frequency Domain. *ACS Appl. Mater. Interfaces* **2019**, *11* (26), 23320−23328.
(27) Courtier, N. E.; Cave, J. M.; Foster, J. M.; Walker, A. B.; Richardson, G. How Transport Layer Properties Affect Perovskite Solar Cell Performance: Insights from a Coupled Charge Transport/Ion Migration Model. *Energy Environ. Sci.* **2019**, *12* (1), 396−409.
(28) Jacobs, D. A.; Wu, Y.; Shen, H.; Barugkin, C.; Beck, F. J.; White, T. P.; Weber, K.; Catchpole, K. R. Hysteresis Phenomena in Perovskite Solar Cells: The Many and Varied Effects of Ionic Accumulation. *Phys. Chem. Chem. Phys.* **2017**, *19* (4), 3094−3103.
(29) Chang, T.-C.; Liao, C.-Y.; Lee, C.-T.; Lee, H.-Y. Investigation of the Performance of Perovskite Solar Cells with ZnO-Covered PC61BM Electron Transport Layer. *Materials* **2023**, *16* (14), 5061.
(30) Wu, F.; Lu, S.; Hu, C.; Lu, H.; Chen, C.; Tang, J.; Yang, S.; Zhu, L. A Smart Way to Prepare Solution-Processed and Annealing-Free PCBM Electron Transporting Layer for Perovskite Solar Cells. *Adv. Sustainable Syst.* **2022**, *6* (9), 2200212.
(31) Uddin, M. A.; Rana, P. J. S.; Ni, Z.; Dai, X.; Yu, Z.; Shi, Z.; Jiao, H.; Huang, J. Blading of Conformal Electron-Transport Layers in p−i−n Perovskite Solar Cells. *Adv. Mater.* **2022**, *34* (30), 2202954.
(32) SILVACO, Inc.. *ATLAS User's Manual Device Simulation Software*, 2016.
(33) Wu, F.; Bahrami, B.; Chen, K.; Mabrouk, S.; Pathak, R.; Tong, Y.; Li, X.; Zhang, T.; Jian, R.; Qiao, Q. Bias-Dependent Normal and Inverted J−V Hysteresis in Perovskite Solar Cells. *ACS Appl. Mater. Interfaces* **2018**, *10* (30), 25604−25613.
(34) Li, C.; Tscheuschner, S.; Paulus, F.; Hopkinson, P. E.; Kießling, J.; Köhler, A.; Vaynzof, Y.; Huettner, S. Iodine Migration and Its Effect on Hysteresis in Perovskite Solar Cells. *Adv. Mater.* **2016**, *28* (12), 2446−2454.

https://doi.org/10.1021/acsaem.4c01993
ACS Appl. Energy Mater. 2025, 8, 759−766